Discover Chemistry

RESEARCH Open Access

Utilization of *Cuscuta japonica* powder as a novel affordable adsorbent for removing disperse dyes from water

Nebert Shiyoya[1], Rahab Kamau[1] and Gershom Mutua[1*]

*Correspondence:
Gershom Mutua
gmutua@mmust.ac.ke
[1]Department of Pure and Applied Chemistry, School of Natural Sciences, Masinde Muliro University of Science and Technology, P.O Box 190, Kakamega 50100, Kenya

Abstract

Textile industrial activities have become major contributors of water pollution through the release of dyes into water systems. Disperse red 13 and disperse orange 3 dyes are still heavily used in the industry despite having been reported to be carcinogenic. Adsorption using locally available materials has recently emerged as an effective technology for the removal of pollutants from water. In this study, the potential of *Cuscuta japonica* powder was investigated for the removal of disperse red 13 and disperse orange 3 dyes from water. The *C. japonica* powder's functional groups and the surface chemistry were examined using FTIR spectroscopy and SEM, respectively. TG-DTG analyses were employed to study the thermal characteristics of the powder while EDS was used to determine the elemental composition profile of the powder. Experiments were performed to determine the effect of contact time, pH, initial adsorbate concentration and reaction temperature on the removal of the two dyes from aqueous solution. After 120 min of reaction at 25 ℃, the removal efficiencies recorded were 87.77% and 79.16% for disperse red 13 and disperse orange 3, respectively. The corresponding sorption capacities were 11.10 mg/g for disperse red 13 and 10.61 mg/g for disperse orange 3. The adsorption of the two dyes onto the *C. japonica* powder followed the *pseudo*-second order kinetic model. This indicates that the adsorption of the two dyes is largely chemisorption. The Sips isothermal model provided the most appropriate fit for the two dyes. The adsorption of the two dyes onto the powder occur mainly through π–π stacking, hydrophobic interactions, and hydrogen bonding. The adsorption reaction of two dyes onto the adsorbent was exothermic and spontaneous. It was also established that the powder can be used more than three times without significantly losing its adsorptive capacity. These findings demonstrate that *C. japonica* vines can serve as an affordable source for adsorbent materials for the remediation of water polluted with industrial dyes.

Keywords Adsorption, C. japonica, Disperse dyes, Isotherms, Kinetics, Thermodynamics

1 Introduction

Water constitutes over 71% of the earth's surface and is an important resource for all living species. In recent years, population growth and industrial development have intensified both its consumption and pollution [1]. Among the major pollutants, synthetic dyes from the textile sector pose serious health and environmental risks because of their chemical stability and resistance to conventional treatment methods [2]. Disperse dyes, such as Disperse Red 13 (DR13) and Disperse Orange 3 (DO3) are particularly of great concern. Their aromatic and azo structures make them highly persistent, and during degradation they release toxic aromatic amines associated with carcinogenicity and mutagenicity [3]. Exposure to synthetic dyes such as DR13 and DO3 has also been linked to respiratory disorders, skin irritation, reproductive complications, allergic reactions and impairment of the nervous system [4]. Even at low concentrations, dyes impair the visual quality of water, hinder light penetration, and may bio-accumulate through the food chain, thereby amplifying their ecological and health effects [5].

Several treatment methods have been used to mitigate dye-containing effluents, but their efficiency remains limited. For instance, chemical approaches such as advanced oxidation, ozonation and reverse osmosis can degrade dyes but often generate secondary pollutants. They also require intensive energy for operation [6]. Biological treatments are friendly to the environment but are slow and ineffective for non-biodegradable dyes like disperse dyes [7]. Similarly, physical methods such as coagulation-flocculation and membrane filtration offer moderate effectiveness although they are often limited due to their high costs of operation and the generation of sludge [8]. Adsorption is the most effective technique for the removal of dyes from water due to its affordability, simplicity, reusability of the adsorbents, and can remove dye molecules completely without leaving toxic moieties [9].

The search for alternative and economically viable adsorbents for wastewater treatment has increasingly focused on the use of locally available materials. The affordability, biodegradability, sustainability and environmental friendliness of these materials make them more appealing [10]. Although activated carbon is one of the heavily utilized adsorbent, its application is limited by its high cost and poor regeneration capacity [11]. To address this, various adsorbents has been studied for their potential in removing dyes from aqueous solutions. These include, biomass and agricultural wastes [12, 13], natural clays [14], and industrial waste materials [15]. Among these, lignocellulosic materials have shown considerable potential for removing dyes because of their porous structure, availability, and abundance of functional groups. Reported examples include sawdust [16], fruit peels [17, 18], plant leaves [19], maize cobs [20], and coconut husks among others [21].

This work investigated the applicability of *Cuscuta japonica* powder as an affordable and environmentally sustainable bio-sorbent for the removal of DR13 and DO3 from water. *C. japonica* commonly known as dodder is a wild sessile and parasitic plant. Harnessing this widespread and invasive species for pollutant removal offers both economic value and environmental sustainability. However, data on its suitability for the remediation of polluted water is limited. Although, it was recently reported to remove atrazine and diuron from water achieving efficiencies of 85 and 79%, respectively [22]. Furthermore, no reports are available on its capability to remove dyes from water. In fact, this is the first study to report the use of *C. japonica* in adsorptive removal of dyes from water.

Adsorptive performance of the *C. japonica* powder was assessed through a laboratory study by examining the effects of reaction contact time, pH, initial dye concentration, and temperature. Adsorption kinetics was examined using *pseudo*-first order, *pseudo*-second order, intraparticle diffusion and Elovich models while equilibrium data were fitted to the Langmuir, Freundlich, Sips and Temkin isotherm models. Thermodynamic properties of the adsorption process were determined by varying the reaction temperature. The findings provide invaluable data on the efficiency and applicability of *C. japonica* as a bio-sorbent highlighting its potential in scale-up for water treatment.

2 Materials and methods

2.1 Materials

Reference standards for Disperse Red 13 (95%) and Disperse Orange 3 (90%) were procured from Merck Pty. Sodium hydroxide (98%), Hydrochloric acid (37%) and deionized water were supplied by Kobian Kenya Ltd. *Cuscuta japonica* vines were collected in July 2024 in Lurambi area (0.323° N, 34.77° E) in Kakamega County, Kenya. The plant material was identified by Ms. Consolata Shilaho, a taxonomist based at Masinde Muliro University of Science and Technology. The voucher specimen was deposited at the University Herbarium with ID NS/KK/01/2024.

Cuscuta japonica was used as an adsorbent of choice in this study due to its abundant availability which makes it a low-cost and sustainable material. The plant is fibrous with lignocellulosic structure rich in different functional groups that can interact with the adsorbate molecules, making it suitable for adsorption studies. Due to its widespread, *C. japonica* offers an eco-friendly alternative that can be collected at low cost and easily processed for water treatment.

2.2 Preparation of the adsorbent

The harvested vines were cleaned with deionized water, air-dried at ambient conditions before being finely ground using a mechanical grinder. To eliminate surface and soluble impurities, the resulting powder was thoroughly cleaned with copious amount of deionized water until the filtrate was clear. The cleaned sample was then oven-dried at 100 ℃ for 24 h. The dried material was subsequently passed through a 200 µm mesh sieve to attain uniform particle size suitable for adsorption studies. Surface activation of the adsorbent was carried out according to Bulimo et al. (2024) [22], in which the milled material was immersed in 0.1 M HCl for 24 h. After that, deionized water was used to rinse the adsorbent continually until the pH of the wash water reached neutral. It was again oven-dried at 100 ℃ and stored in a tightly sealed container before use.

2.3 Characterization of adsorbent

The surface characteristics of the activated C. *japonica* powder was examined using Scanning electron microscopy (SEM) (JEOL JSM 6701 F, model) while the elemental profile of the powder was studied by Energy Dispersive X-ray spectroscopy (EDS). The powder was placed on carbon sticky tape to prevent movement and coated with a fine layer of gold to make it more conductive and produce better images. The measurements were taken using electron beam with energy of 20 kV [23]. The functional groups present in the powder were determined using a Perkin-Elmer Fourier transform infrared (FTIR) spectrometer between 4000 and 400 cm^{-1}. The thermal properties of the adsorbent were

determined using Mettler Toledo TGA 2 Stare System. The point of zero charge (pH_pzc) of the powder was determined by the salt-addition method as described in literature [24].

2.4 Batch experiment

Stock solutions of 50.0 ppm were prepared for each dye using deionized water in 500 mL volumetric flask. From the stock solutions, a series of standard working solutions were prepared by dilution using deionized water. Adsorption studies were monitored spectrophotometrically using UV 1609 UV/VIS Spectrophotometer at 520 and 440 nm for DR13 and DO3, respectively.

Calibration curves were obtained by plotting the absorbance of different concentration (three replicates) of the dyes. The calibration curves are shown in Fig. SI 1 (Supplementary Information). The resulting calibration curves were linear over the tested concentration ranges (5–30 ppm) indicating a direct proportional relationship between absorbance and concentration as expected under the Beer Lambert law [25]. The coefficients of determination (R^2) were found to be 0.9992 and 0.9984 for DR13 and DO3, respectively. These calibration curves were subsequently used to compute unknown dye concentrations from the experiments.

All the experiments were performed using 50 mL of the adsorbate solution in 250 mL conical flasks in a temperature-controlled shaker at an agitation speed of 150 rpm. To determine the effect of reaction time, 0.2 g of the adsorbent were contacted with 10 ppm solution at 298 K. After specific reaction time (5, 10, 15, 30, 45, 60, 75 and 120 min), the residual concentration of the dyes in the solution was determined. The influence of initial concentration of the two dyes was assessed by varying the adsorbate concentrations (5, 10, 15, 20, 25 and 30 ppm) while keeping other conditions constant (adsorbent dose of 0.2 g, temperature of 298 K and reaction time of 60 min). The effect was conducted by varying the pH of the reaction solution while the other conditions constant. The pH of the solution was varied from 2 to 10 using 0.1 M HCl and NaOH solutions. Thermodynamic results were generated by performing the reactions at four different temperatures (298, 303, 308 and 313 K) while keeping all other conditions constant (adsorbent amount of 0.2 g, contact time of 60 min and 10 ppm solution). All experiments utilized solutions prepared using the dye reference standards [24]. Freshly prepared solutions were used in all the experiments. All the reactions were monitored in triplicates. Deionized water was used for the blank experiments. To further to ensure validity of the results, inter-day and intra-day monitoring of absorbance was done.

The percent removal of the dye by the adsorbent (%R) was determine as shown in Eq. 1

$$dyes\ removal\ \ (\%) = \frac{(C_i - C_e)}{C_i} \times 100 \tag{1}$$

Key: C_i; starting concentration of the dye, C_e; concentration remaining at equilibrium, both in mg/L.

The equilibrium dye uptake (q_e) by the *C. japonica* powder at equilibrium per unit mass was computed according to Eq. 2

$$q_e = \frac{(C_i - C_e)\,V}{M} \tag{2}$$

Key: V; solution volume (L) used, M; quantity of the powder used (g) [26].

2.5 Kinetic study

Adsorption kinetics of DR13 and DO3 onto the *C. japonica* powder was modelled using four different non-linearized models; *pseudo*-first order (Eq. 3), *pseudo*-second order (Eq. 4), Elovich (Eq. 5) and the Intraparticle diffusion (Eq. 6) [27–29].

$$q_t = q_e\left(1 - e^{-k_1 t}\right) \tag{3}$$

Key: q_t*; adsorption capacity (mg/g) at time t,* q_e *; equilibrium adsorption capacity (mg/g),* k_1*; rate constant (min*$^{-1}$*).*

$$q_t = \frac{k_2 q2_e}{1 + k_2 q_t} t \tag{4}$$

Key: $q2_e$*; amount adsorbed (mg/g) at equilibrium,* q_t *; the amount adsorbed (mg/g) at time t,* k_2 *; rate constant (g mg*$^{-1}$ *min*$^{-1}$*).*

$$q_t = \frac{1}{\beta}\ln(\alpha\beta) + \frac{1}{\beta}\ln(t) \tag{5}$$

Key: α*; initial adsorption rate (mg g*$^{-1}$*min*$^{-1}$*),* β*; relates to surface coverage and activation energy for chemisorption (g mg*$^{-1}$*).*

$$q_t = K_P\, t^{0.5} + C \tag{6}$$

Key: K_P *;intra-particle diffusion,* C*; rate constant.*

2.6 Adsorption isotherm modeling

Adsorption isotherms describe how the adsorbate is distributed at equilibrium on the solid sorbent at a constant temperature. They provide valuable information for designing and optimizing adsorption processes [30]. This study used four different isothermal models; Langmuir (Eq. 7), Freundlich (Eq. 8), Temkin (Eq. 9) [31] and Sips (Eq. 10) [32]

$$q_e = \frac{q_{max} K_L C_e}{1 + K_L C_e} \tag{7}$$

Key: Ce; equilibrium concentration (mg/L), q_e*; quantity of dye adsorbed at equilibrium (mg g*$^{-1}$*),* q_{max}*; maximum adsorption capacity (mg/g),* K_L*; binding affinity (L /mg).*

$$q_e = K_f\ (C_e\ ) \tag{8}$$

Key: K_f*; adsorption capacity, n; adsorption intensity.*

$$q_e = \frac{RT}{B_T}\ln(A_T C_e) \tag{9}$$

Key; B_T*; Temkin heat of sorption (J/mol),* A_T*; Equilibrium binding constant (L/g), T; temperature (K).*

$$q_e = \frac{q_s\ K_s C_e^n}{(1 + K_s C_e^n)} \tag{10}$$

Key; q_s*,* K_s *and n are isotherm constants. n represents heterogeneity index. The greater the n value is, the more heterogeneous the system is said to be.*

2.7 Thermodynamics study

To understand the nature and energy changes during adsorption, and the applicability of the adsorbent, $\Delta G, \Delta H$ and ΔS were computed. The change in Gibbs free energy (ΔG) was calculated using Eq. 11 [31]

$$\Delta G = -RTlnk_c \tag{11}$$

Where $k_c = \frac{q_e}{C_e}$

ΔH and ΔS were obtained from Van't Hoff plots of lnk_c against $\frac{1}{T}$ as expressed by Eq. 12.

$$lnK_c = -\frac{\Delta H}{RT} + \frac{\Delta S}{T} \tag{12}$$

2.8 Statistical analysis

The data obtained from this study was processed and analyzed using Origin 2019 software. The model's suitability was assessed using statistical parameters such as coefficient of determination (R^2) and error analysis metrics (sum of squared errors (SSE) and Chi-square (χ^2)). These error functions are important in selecting the most suitable model by minimizing deviations between experimental and predicted values [33].

3 Results and discussion

3.1 Characterization of the activated *C. japonica* powder

3.1.1 Scanning electron microscopic analysis

The surface topography and structural properties of *C. japonica* powder were analyzed using SEM. Figure 1 present images at magnification of x500 (a) and x1000 (b), revealing the texture and physical structure of the adsorbent. The micrographs confirmed the heterogeneity of the surface by showing spaced sheets that have pores and cavities. The

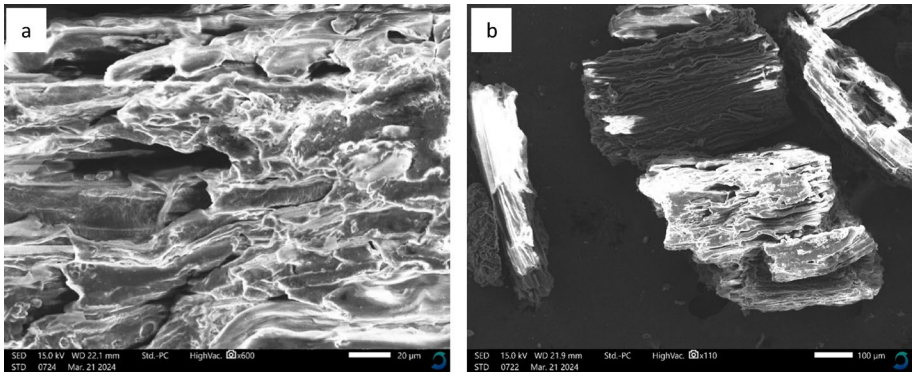

Fig. 1 Morphology of *C. japonica* powder as observed through SEM at x500 (a) and x1000 (b)

nature of the sheets increases the surface area providing opportunity for the attachment of the dye molecules through adsorption. The adsorbent's surface is characterized by voids and roughness which enhances the interaction and dispersion of the adsorbates into the pores where they are adsorbed on the active sites [34].

3.2 EDS analysis

The EDS analysis provided a comprehensive elemental composition of the *C. japonica* powder. Figure 2 revealed that the adsorbent's surface contains carbon (about 61%) oxygen (about 38%) and small amounts of Calcium and Potassium.

The carbon and oxygen likely originate from carbohydrates and lignin, which are present in the plant materials. These chemical metabolites bear the functional groups like the aliphatic and aromatic hydroxyl, carboxyl, methoxyl and amine. This is supported by the FTIR results. These functional groups are important in the surface chemistry of the powder for its use as an adsorbent for the removal of the selected dyes from aqueous solutions [19, 20].

3.3 Fourier transform infrared (FTIR) spectroscopic analysis

The 4000 –400 cm^{-1} FTIR spectrum of the powdered *C. japonica* was obtained and is displayed in Fig. 3.

The broad peak at 3425 cm^{-1} is attributable –OH stretch interpreted for hydrogen bonded hydroxyl groups for alcohols and phenols in the powder [35]. The absorption bands observed at 2855 and 2922 cm^{-1} corresponds to stretching vibration of aliphatic C-H groups, indicating the presence of alkanes on the surface of the adsorbent [36]. A minor absorption peak at 1734 cm^{-1} is characteristic for pectin in the cellulose. Furthermore, the peak at 1637 cm^{-1} represents –N-H bend, a functional group for primary amines [37]. In addition, medium peaks at 1420 and 1398 cm^{-1} represent a -C-C stretch, while that at 1334 cm^{-1} is assigned to -C-N stretch for aromatics [38]. The presence of amine groups in the *C. japonica* was further supported by strong bands at 1110 and 1035 cm^{-1} reflecting -C–N stretches and at 909 cm^{-1} interpreted for –N-H wag for primary amines [39]. The peaks at 744–831 are attributed to N-H deformation of amine [40]. The

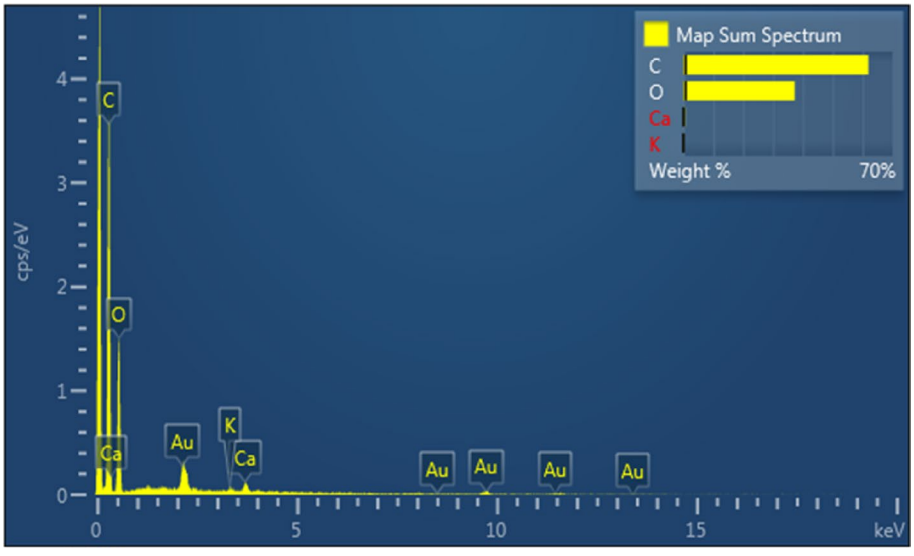

Fig. 2 EDS elemental composition for *C. japonica* powder

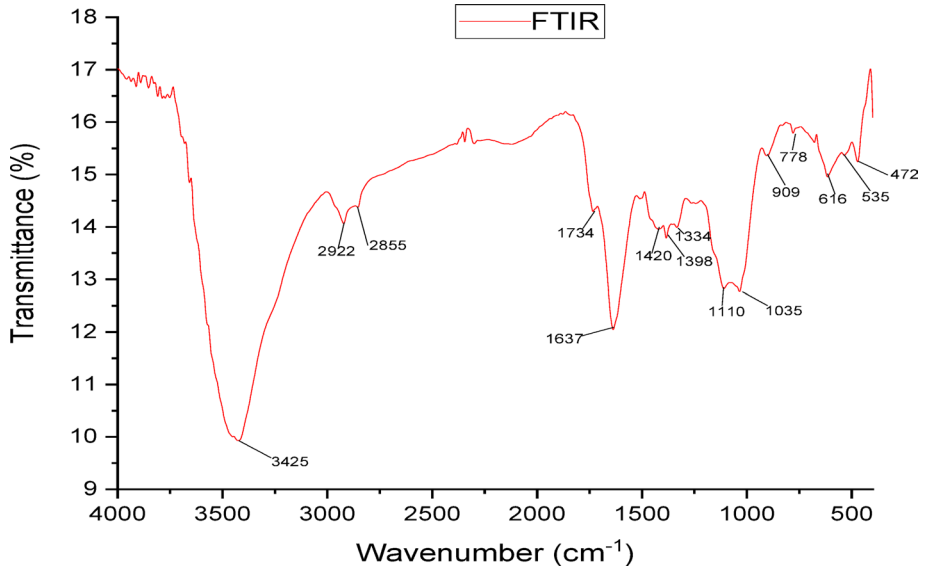

Fig. 3 4000–400 cm^{-1} FTIR spectrum of *C. japonica* powder

band at 616 cm^{-1} may correspond to C-O-H deformation or skeletal vibration. The peaks at 778 and 535 cm^{-1} are attributable to bending vibration of C-H while the peak at 472 cm^{-1} is attributable to bending vibrations of C-O-C and C-O-H [41].

3.4 Thermogravimetric analysis

Thermogravimetric (TG) and derivative thermogravimetric (DTG) analyses are useful in evaluating the stability and decomposition behavior of the adsorbent by monitoring the change in mass as a function of temperature. The TG-DTG curves of the *C. japonica* powder is shown in Fig. 4. TG analysis determines how the mass of the material changes when it is subjected to heating. This provides an insight into moisture content loss, volatile release and thermal decomposition profile of the material. It can also reveal the decomposition of non-carbonaceous components. On the other hand, DTG curve displays the rate of mass loss with respect to temperature [42].

From Fig. 4, the TG curve of *C. japonica* powder exhibited multiple weight loss stages. An initial weight 5–10% loss occurred between 50 and 200 °C due to moisture evaporation [43]. The second mass loss of 50–60% occurred between 200 and 400 °C as a result of the decomposition of cellulose, hemicellulose and lignin [44]. The gradual mass loss observed from 400 to 600 °C is due to the breakdown of carbonaceous materials in the powder. A final minor weight loss of 5% between 600 and 800 °C corresponds to residual carbon oxidation, leaving behind ash. The DTG curve provides a clearer view of these transitions, with distinct peaks: a small one at 50–150 °C for moisture removal, a sharp peak between 300 and 350 °C indicating cellulose and hemicellulose degradation, and broader peaks between 400 and 600 °C representing lignin decomposition [45]. These results show that the sorbent is thermally stable at the temperatures adopted for the adsorption experiment.

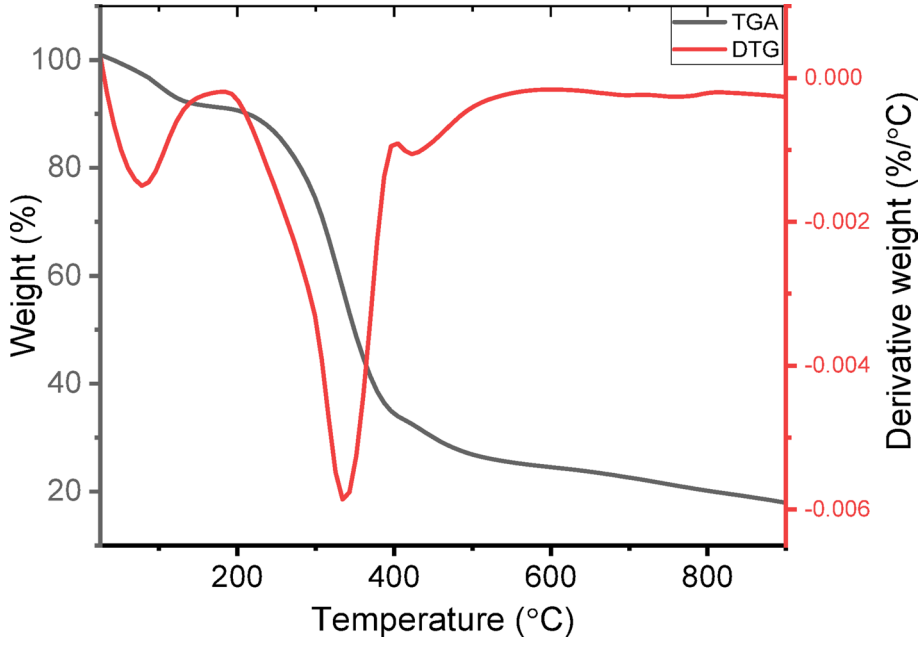

Fig. 4 TG and DTG curves for the *C. japonica* powder

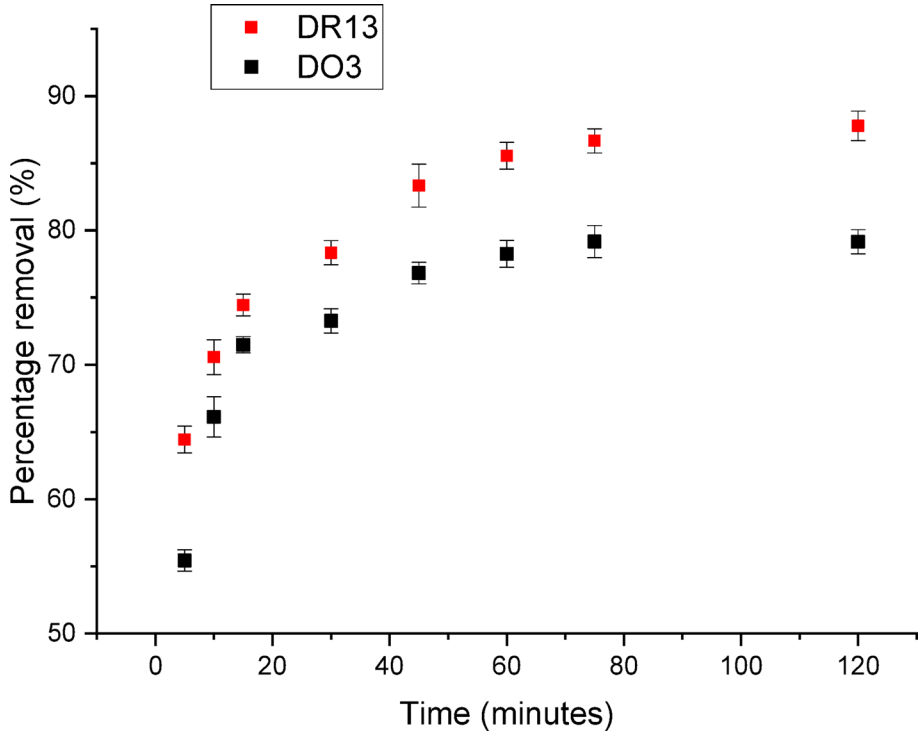

Fig. 5 Percent removal of DR13 and DO3 by *C. japonica* powder as function of reaction time

3.5 Adsorption studies

3.5.1 Effect of reaction contact time

To determine the extent to which contact time affects adsorption capacity, the samples were subjected to experimental duration ranging from 5 to 120 min. As shown in Fig. 5,

the highest percent removal of dyes was 87.77% for DR13 and 79.16% for DO3 after 120 min.

The percent removal increased rapidly during the preliminary phase of the reaction, reaching equilibrium uptake within 60 min for the two disperse dyes. This increase can be linked to the presence of abundant unoccupied sites on the adsorbent's surface allowing efficient interaction between the adsorbates and the active binding sites [46]. In addition, the adsorption of the dye molecules can be associated with their interaction with various functional groups on the surface of the adsorbent as evidenced by FTIR analysis. The percent removal of DR13 was higher than that DO3 despite it having a larger molar mass of 348.78 g/mol compared to 242.23 g/mol of DO3. This is likely due to its various functional groups which promote stronger interactions with the adsorbent.

However, beyond the optimal time (60 min), the rate of adsorption gradually declined and no significant changes were observed. The reduction in the rate of dye removal can be due to the system reaching equilibrium as well as the saturation of the active sites which impedes further adsorption [47]. The subsequent adsorption reactions were therefore monitored for 60 min.

3.6 Effect of initial concentration

A key aspect that significantly affects adsorption capacity is the initial pollutant concentration. In the current study, the concentrations used were 5, 10, 15, 20 and 30 mg/L. According to Fig. 6, the amount sorbed improved with rising dye concentration, as indicated by rise in adsorption capacity from 1.28 to 4.71 mg/g for DR13 and from 1.89 to 6.86 mg/g for DO3. The reason for this is that as the concentration was increased the concentration gradient pushed the mass transfer process to overcome resistance [48]. When dye is present at low concentration, the powder has more available sites for adsorption which facilitates the uptake of the dye molecules. However, when there are more dye molecules present in the solution, there is a high competition for the adsorption sites leading to saturation. This reduces the overall percent removal [49]. Specifically, for DR13, the adsorption percent decreased from 89.6 to 61.6% and for DO3, from 85.4 to 59.1%. Sudarsan and coworkers (2025) reported a similar observation, where the removal efficiency of Congo red from water using activated carbon obtained from *Spathodea campanulata* flowers reduced from 84.05 to 46.56% when the dye concentration was increased from 20 to 60 mg/L [50].

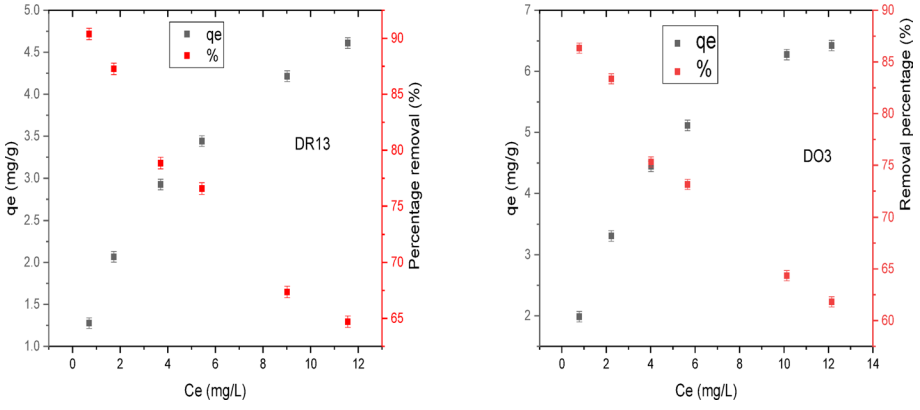

Fig. 6 Removal of DR13 and DO3 by *C. japonica* powder as a function of initial dye concentration

3.7 Effect of pH

pH of the reaction solution is an important parameter that can alter the charge on the surface of an adsorbent, thereby affecting adsorption efficiency [51]. The effect of pH on the removal of DR13 and DO3 was studied by varying the reaction solution pH from 3 to 10. Figure 7 shows the percent removal of the dyes as a function of pH, measured at a constant contact time of 60 min, an adsorbent mass of 0.2 g, and a dye concentration of 10 mg/L and a temperature of 298 K.

It was observed that the removal efficiency remained almost constant between pH 3 and 6 for DR13 showing that the adsorption process in this range is largely independent of solution pH. Such stability can be attributed to π–π stacking, hydrogen bonding and van der Waals interactions between the dye molecules and the functional groups on the surface of the adsorbent. On the other hand, the removal efficiency of DO3 showed a slight increase within the same pH range. This may be attributed to alteration of charge distribution and hydrophobic character of the dye [52].

DR13 and DO3 are nonionic in nature, lacking sulfonate or quaternary groups that typically drive strong electrostatic interactions. Nevertheless, their polar substituents may undergo protonation under acidic conditions, introducing partial positive charges that further support adsorption. Beyond pH 6, the percent removal gradually declined for the two dyes. As shown in Fig. 8, the point of zero charge (pHpzc) of the powder was 6.0. At pH values below this point, the surface remains positively charged, which favors weak interactions with protonated dye substituents and helps sustain adsorption. Beyond pH 6, the adsorbent surface becomes increasingly negatively charged. Since DR13 and DO3 are nonionic, this does not lead to strong electrostatic repulsion. Instead, the negative surface charge decreases the availability of hydrogen bonding sites and weakens interactions with the adsorbates. Additionally, the presence of excess hydroxyl

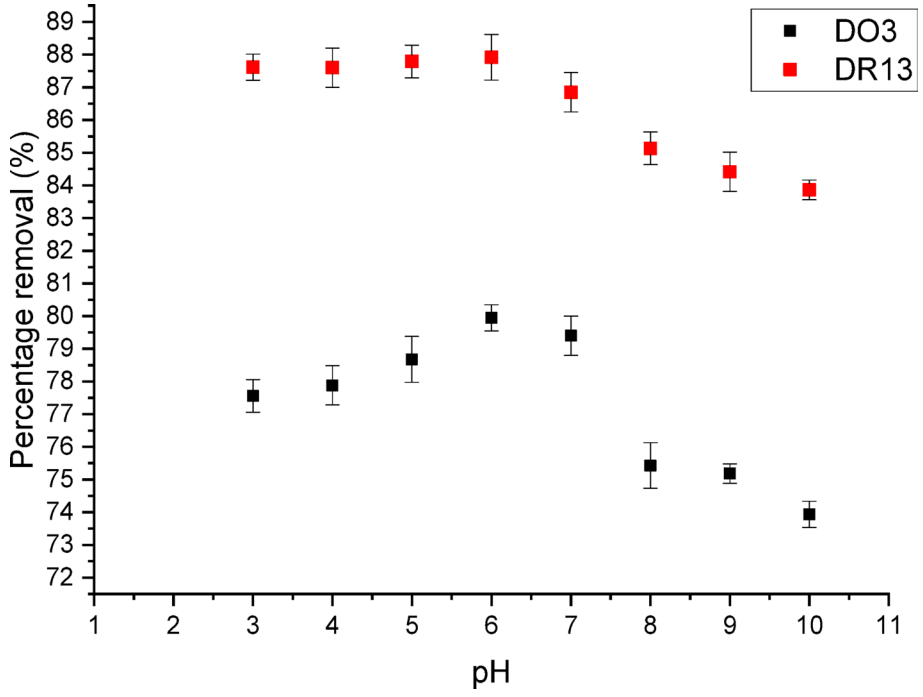

Fig. 7 Effect of pH on the removal of DR13 and DO3

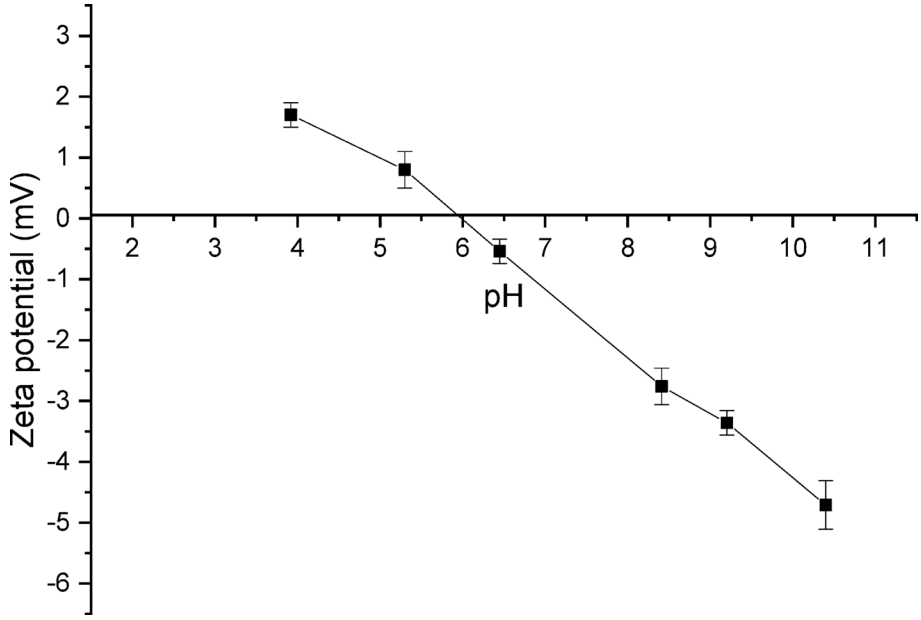

Fig. 8 A plot showing the point of zero charge of *C. japonica* powder

ions at higher pH may interfere with hydrogen bonding and weakly compete with dyes for sorption sites, decreasing the removal efficiency further [53].

DR13 and DO3 are disperse azo dyes composed of large aromatic backbones with azo linkages (–N = N–), along with polar substituents such as nitro ($–NO_2$) and amino ($–NH_2$) groups. These polar heads confer some degree of polarity, aiding dispersion in water. As a result, the dyes exist largely as suspended particles or aggregates, and adsorption is governed primarily by π–π stacking, hydrophobic interactions, and hydrogen bonding rather than strong electrostatic attraction.

In this study, the adsorption studies were carried out at neutral pH because we intent to apply the powder in wastewater treatment under natural environmental conditions.

3.8 Effect of temperature

Reaction temperature plays a significant role in determining the efficiency and applicability of an adsorbent, since it influences the extent to which the adsorbate binds on the adsorbent. In this work, the adsorptive removal of the two dyes was carried at four different temperatures (298, 303, 308 and 313 K). Figure 9 shows that the quantity of dye adsorbed decreased when the reaction temperature was raised showing that the adsorption process was exothermic.

In regard to this, increasing the reaction temperature causes the dye molecules to acquire more kinetic energy which reduces their likelihood of adhering to the adsorbent [54]. In addition, higher temperatures may also weaken the physical structures of the dyes which further decreases the efficiency of the adsorption process [55]. Such processes are common in physisorption and are marked by the interaction of adsorbent and adsorbate mainly through electrostatic attraction and van der Waals forces. This proves that the bond between the molecules and the sorbent surface is stronger at lower temperatures [56]. A similar observation on the effect of temperature on disperse dyes was reported by Tiwari and coworker (2015) [57].

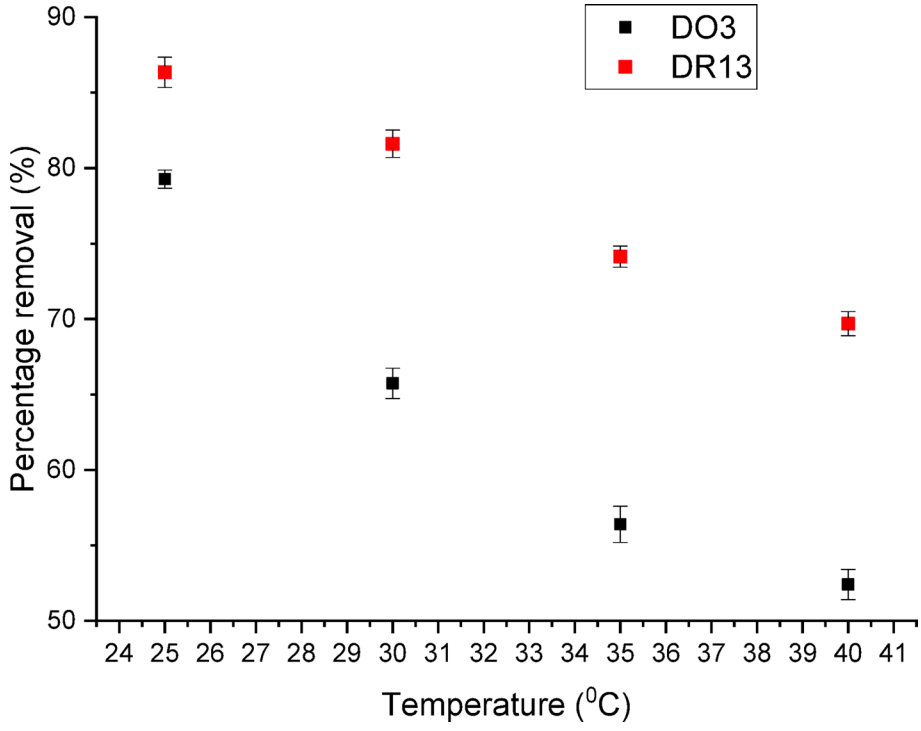

Fig. 9 Removal efficiencies of DR13 and DO3 as a function of reaction temperature

Table 1 Kinetic results obtained for the adsorptive removal of DR13 and DO3 by *C. japonica* powder

Model	Parameter	DR 13	DO 3
Pseudo-first order	Qe (mg/g)	2.061 ± 0.053	3.046 ± 0.054
	(k_1) (min^{-1})	0.241 ± 0.038	0.309 ± 0.042
	$(R_{adj})^2$	0.672	0.694
	χ^2	0.0157	0.018
	SSE	0.094	0.108
Pseudo-second order	Qe (mg/g)	2.179 ± 0.028	3.159 ± 0.025
	K_2 (g/mg min)	0.207 ± 0.025	0.126 ± 0.009
	$(R_{adj})^2$	0.949	0.957
	χ^2	0.0024	0.0025
	SSE	0.0145	0.0151
Intra-particle diffusion	K_{diff}(mg/g $min^{-0.5}$)	0.068 ± 0.021	0.077 ± 0.021
	C	1.540 ± 0.338	2.472 ± 0.086
	$(R_{adj})^2$	0.843	0.834
	χ^2	0.0075	0.0269
	SSE	0.0450	0.0161
Elovich	α (mg/g.min)	131.559 ± 9.34	256.384 ± 20.7
	β (g/mg)	5.049 ± 0.32	4.459 ± 0.31
	$(R_{adj})^2$	0.9699	0.9701
	χ^2	0.0014	0.0018
	SSE	0.0086	0.0106

3.9 Kinetic modeling

To assess the kinetics of DR13 and DO3 the following models were applied: *pseudo*-first order, *pseudo*-second order, intra-particle and Elovich. The results are presented in Table 1 while the fittings are displayed in Fig. SI 2 (Supplementary Information).

The *pseudo* first order model is centered on the postulation that the rate of adsorption is proportionate to the vacant sorption sites [58]. For DR13, the calculated equilibrium adsorption capacity (Q_e) was 2.061 ± 0.053 mg/g with a rate constant (k1) of 0.241 ± 0.038 min^{-1}, whereas DO3 showed a higher Q_e of 3.046 ± 0.054 mg/g and a k1 value of 0.309 ± 0.042 min^{-1}. However, the model exhibited a poor fit for both dyes with an adjusted R^2 of 0.6715 for DR13 and 0.6943 for DO3. The relatively high sum of squared errors (SSE) of 0.094 for DR13 and 0.108 for DO3, together with chi-square (χ^2) of 0.0157 and 0.018 for DR13 and DO3, respectively further showing that this model does not adequately describe the adsorptive kinetic behavior of the two dyes. The poor performance of *pseudo* first order suggests that adsorption is not governed by a simple physisorption process or diffusion-limited process but rather by chemisorption interactions. This interpretation is supported by the heterogeneous nature of *C. japonica*, as revealed by SEM images showing rough, irregular surfaces with varying pore sizes (Fig. 1). Similar deviations have also been reported in previous studies, where heterogeneous surface chemistry limited the applicability of the *pseudo*-first order model. This likely results from dye molecules adhering to active surface sites through chemical bond formation [59].

From the results, the *pseudo*-second order model fitted the kinetic data better compared to the *pseudo*-first order and the intra-particle diffusion models. This is evidenced by the high R^2 values of 0.949 and 0.957 for DR13 and DO3, respectively, as well as low corresponding χ^2 values of 0.0024 and 0.0025. In addition, the model recorded low SSE values of 0.0145 and 0.0151 for DR13 and DO3, respectively. This indicates that chemisorption is the rate-limiting step, involving electron sharing or electron exchange between dye molecules and the functional groups on the powder's surface [60]. DR13 exhibited a higher adsorption rate constant (0.207 ± 0.025 g/mg·min) compared to DO3 (0.126 ± 0.009 g/mg·min), implying a faster initial uptake.

The better overall fit for DO3 compared to DR13 indicates stronger and more stable interactions at equilibrium. This outcome is somewhat inconsistent with diffusion expectations, since the smaller DO3 molecule (242.23 g/mol) should, in principle, adsorb faster than the bulkier DR13 (348.78 g/mol). The anomaly can be attributed to preferential surface interactions of DR13 with high-energy sites, possibly through π–π stacking with aromatic moieties. Nonetheless, the smaller size of DO3 allows deeper pore penetration, which explains its stronger equilibrium binding. This behavior is typical in systems where the dye forms strong chemical bonds with the active sites, as observed in other adsorption studies involving azo dyes and lignocellulosic adsorbents [61].

Intra-particle diffusion model was employed to evaluate how internal diffusion resistance and dye molecule diffusion into the adsorbent's pores influence the adsorption process. The results revealed that adsorption of the two dyes onto the powder proceeded in two steps: the first fast step is initial boundary layer diffusion while the second slower one is intra-particle diffusion. The diffusion constants (K_{diff}) were 0.068 ± 0.021 mg/g·$min^{0.5}$ for DR13 and 0.077 ± 0.021 mg/g·$min^{0.5}$ for DO3, indicating that DO3 diffused more rapidly, likely due to its smaller molecular size (242.23 g/mol) compared to DR13 (348.78 g/mol). The non-zero intercepts (C) of 1.540 ± 0.338 for DR13 and 2.472 ± 0.086 for DO3 confirm that intra-particle diffusion was not the sole rate-limiting step; boundary layer resistance also played a role. Since a larger C value reflects a thicker boundary layer, DO3 experienced greater external mass transfer resistance than DR13

role [62]. The R^2 value was higher for DR13 (0.8428) than for DO3 (0.8343), suggesting that intra-particle diffusion contributed slightly more to the removal of DR13. These results agree with earlier documented reports showing that dye molecules undergo adsorption through a multi-step process. It involves both film diffusion and pore diffusion mechanisms [63].

Chemisorption on energetically heterogeneous surfaces is frequently explained by the Elovich model [64]. The adsorption data of the two dyes fitted best in this model achieving R^2 values of 0.9698 for DR13 and 0.9701 for DO3. This is supported further by lowest error values observed (χ^2 = 0.0014 and SSE = 0.0086 for DR13 and χ^2 =0.0018 and SSE = 0.0106 for DO3). The initial adsorption rate (α) was high for the two dyes recording values of 131.6 mg/g·min for DR13 and 256.4 mg/g·min for DO3. The larger value obtained for DO3 indicate that its initial uptake is more rapid compared to DR13. The β constants were 5.05 g mg^{-1} for DR13 and 4.46 g mg^{-1} for DO3. The slightly lower β for DO3 suggests a slower decline in adsorption rate and thus a comparatively stronger interaction with the adsorbent. These findings support the view that the heterogeneous surface of *C. japonica* powder provides diverse active sites that facilitate chemisorption. Similar findings have been reported by Hoa et al. (2025) where the initial rate was higher than desorption rate confirming an excellent fit to the Elovich model on a heterogeneous surface and diffusion-controlled mechanism [65].

3.10 Adsorption isotherms

Table 2 shows the adsorption data obtained from the four different isothermal model fittings. The fittings are displayed in Fig. SI 3 (Supplementary Information).

According to the Langmuir model, adsorbate molecules form a monolayer on uniform energy sites and that the sorbed solutes do not interact [66]. From Table 2, DO3 recorded an adsorption capacity (q_{max}) of 7.959 ± 0.334 mg/g, which is greater than that

Table 2 Adsorption isotherm data for DO3 and DR13

Model	Parameter	DO3	DR 13
Langmuir isotherm	q_{max} (mg g^{-1})	7.959 ± 0.334	5.678 ± 0.334
	K_L (L mg^{-1})	0.337 ± 0.042	0.316 ± 0.053
	R_L	0.029	0.031
	$(R_{adj})^2$	0.987	0.980
	χ^2	0.040	0.033
	SSE	0.158	0.131
Freundlich isotherm	K_F (mg g^{-1})	2.441 ± 0.139	1.623 ± 0.049
	1/n	0.402 ± 0.173	0.4327 ± 0.15
	$(R_{adj})^2$	0.984	0.989
	χ^2	0.049	0.006
	SSE	0.196	0.026
Temkin isotherm	q_{max} (mg g^{-1})	3.706 ± 0.512	3.639 ± 0.611
	$(R_{adj})^2$	0.989	0.982
	χ^2	0.034	0.029
	SSE	0.135	0.116
Sips	q_{max} (mg g^{-1})	10.608 ± 0.112	11.097 ± 0.209
	K_S (L mg^{-1})	0.266 ± 0.040	0.163 ± 0.008
	ns	0.717 ± 0.076	0.601 ± 0.011
	$(R_{adj})^2$	0.996	0.999
	χ^2	0.0094	1.053×10^{-4}
	SSE	0.028	3.158×10^{-4}

of DR13 (5.678 ± 0.334 mg/g). This suggests that DO3 has a higher binding affinity and stronger adsorption interaction with the adsorbent likely due to its smaller molecular weight making it fit better into the adsorbent's active sites. Similarily, DO3 recorded a higher K_L value (0.337 ± 0.042 L/mg) compared to DR13 (0.316 ± 0.053 L/mg), indicating a slightly more favorable adsorption process for DO3 [34]. The factor $R_{L,}$ an indicator of isotherm's favorability was found to be 0.0288 for DO3 and 0.0307 for DR13. Since both values were within the range $0 < R_L < 1$, adsorption of the two dyes by *C. japonica* was favorable [27]. The goodness-of-fit values further confirm the Langmuir model's suitability, particularly for DO3, with an R^2 of 0.986 and low error terms (χ^2 = 0.0395; SSE = 0.116), suggesting monolayer adsorption behavior. For DR13, although the adjusted R^2 was slightly lower (0.979), it still indicates a strong correlation affirming the model's applicability.

The Freundlich isotherm explains adsorption on non-uniform surfaces and allows for multilayer adsorption [67]. In this study, as shown in Table 2, adsorption constant K_F indicated stronger interaction for DO3 (2.441 ± 0.14 mg/g) compared to DR13 (1.623 ± 0.049 mg/g). The 1/n values for both dyes were less than 1 (0.402 ± 0.17 for DO3 and 0.433 ± 0.15 for DR13), confirming favorable adsorption and suggesting that the adsorption sites are heterogeneous [68]. A strong correlation was also observed between the experimental data and the Freundlich model, with adjusted R^2 values of 0.984 for DO3 and 0.989 for DR13. The model indicates that heterogeneity and multilayer adsorption may be more pronounced for these dyes.

According to the Temkin model, the heat of the adsorption process is inversely proportional to the surface coverage [69]. The model gave q_{max} of 3.706 ± 0.51 mg/g for DO3 and 3.639 ± 0.61 mg/g for DR13 both lower than those predicted by Langmuir. The R^2 values obtained from this model were high for two dyes (0.989 for DO3 and 0.982 for DR13), and the error values were relatively low, particularly for DR13 (χ^2 = 0.029, SSE = 0.116). This indicates that adsorbate–adsorbent interactions are significant, especially for DR13, and supports the presence of surface heterogeneity and varying adsorption energies, likely due to chemical heterogeneity of the adsorbent [70].

The Sips isotherm employs the strengths of both Langmuir and Freundlich models and is frequently used to explain adsorption on heterogeneous surfaces that approach monolayer saturation at higher solute concentrations [71]. For DO3, the Sips model predicted a maximum adsorption capacity (q_{max}) of 10.61 ± 0.11 mg/g, while DR13 exhibited a slightly higher q_{max} of 11.10 ± 0.21 mg/g. These values are substantially greater than those obtained from the Langmuir model (7.96 and 5.68 mg/g for DO3 and DR13, respectively), suggesting that the Sips model better captures the adsorbent's ability to bind the dyes across both low- and high-energy sites. The affinity constants (K_S) were 0.266 ± 0.04 L/mg for DO3 and 0.163 ± 0.008 L/mg for DR13, indicating that DO3 molecules interact more strongly with the high-energy adsorption sites. However, DR13 ultimately achieved the greater overall uptake capacity, confirming that it adsorbed better than DO3 and exhibited superior maximum loading. The ns values of 0.717 ± 0.076 for DO3 and 0.601 ± 0.011 for DR13, both less than unity, confirms adsorption on an energetically heterogeneous surface. A lower ns value indicates greater surface heterogeneity; thus, DR13 adsorption involves a wider distribution of binding energies than DO3. This may be attributed by the fact that DR13, is more relatively bulkier with more functional groups and interacts with a broader range of functional groups and surface

domains on the adsorbent. This agrees with SEM observations of a rough and porous morphology and FTIR evidence of diverse functional groups that provide a spectrum of binding energies. In terms of statistical validity, the Sips model showed excellent agreement with the experimental data, with adjusted determination coefficients of 0.996 for DO3 and 0.999 for DR13. Error analysis further confirmed this, yielding very low values (χ^2 = 0.0094 for DO3 and 1.05 × 10^{-4} for DR13; SSE = 0.028 and 3.16 × 10^{-4}, respectively). These results demonstrate that the Sips model is superior to Langmuir, Freundlich, and Temkin for describing the adsorption of the two dyes. Importantly, although DO3 shows stronger affinity for high-energy sites, DR13 achieved the highest overall adsorption capacity, confirming its superiority in total uptake among the two dyes.

3.11 Thermodynamic results

Various thermodynamic parameters ($\Delta G,\ \Delta S,\ \Delta H$) were determined. ΔH and ΔS of the reaction were determined from the Van't Hoff plots. The plots are displayed in Fig. SI 4 (Supplementary Information) while corresponding thermodynamics results are summarized in Table 3.

The negative ΔG values for the two dyes observed at 298, and 303 K indicated the spontaneity of adsorption of the two dyes onto the *C. japonica* powder. ΔG turned positive as the temperature increased (at 308 and 313 K), revealing that the adsorptive removal is less likely to happen at higher temperatures. Al-asadi et al. (2023) reported a comparable outcome in relation to methylene blue dye sequestration, noting that ΔG became less negative with increasing temperature [72]. The negative enthalpy changes (ΔH = – 61.11 kJ/mol for DR13 and – 39.99 kJ/mol for DO3) further confirm that the process is exothermic and falls within the range typically associated with chemisorption rather than weak physisorption. Both dyes also displayed negative entropy changes (ΔS), reflecting decreased randomness at the solid–solution interface and indicating that dye molecules adopt a more ordered arrangement on the biosorbent surface compared with their initial state in solution [73]. The entropy decrease is more pronounced for DR13 (–202 J/molK) than for DO3 (–132 J/molK). This larger negative ΔS signifies a greater loss of interfacial disorder and is consistent with DR13's more ordered surface packing. Owing to its larger, more planar molecular geometry, this dye can arrange itself into closely packed, highly ordered layers on the *C. japonica* surface, displacing more water molecules and creating a more organized interfacial region. In contrast, the smaller DO3 molecules produce less structural ordering and therefore exhibit a less negative entropy change.

Table 3 Thermodynamic results for adsorption of DR13 and DO3 onto *C. japonica* powder

Dye	Temp (K)	% removal	ΔG (kJ/mol)	ΔH (kJ/mol)	ΔS (J /molK)
DR13	298	86.30	-0.828	-61.11 ± 3.04	-201.89 ± 6.24
	303	80.46	-0.150		
	308	75.87	1.128		
	313	68.96	2.118		
DO3	298	78.13	-0.435	-39.99 ± 2.95	-132.27 ± 4.87
	303	69.19	-0.055		
	308	58.50	0.637		
	313	49.18	1.551		

3.12 Regeneration of the adsorbent

In order to assess economic viability of *C. japonica* powder as an efficient adsorbent, desorption and regeneration tests were conducted. Four desorption cycles were evaluated in batch experiment system using ethanol as eluent. The results, presented in Fig. 10, indicate that the adsorption performance remained relatively stable during the first three cycles, with *C. japonica* showing nearly the same removal efficiency. Following each regeneration, adsorption experiments were conducted under standardized conditions (C_0 = 10 mg/L, contact time 60 min, agitation 150 rpm, 25 °C). For DR13, the initial removal was 87.8%, and efficiency stayed above 84% through the first three cycles before dropping to 75.24% in the fourth. DO3 followed a similar pattern, starting with 79.16%, remaining above 70% for the first three cycles, and then falling to 66.31% by the fourth cycle. This stepwise loss of capacity indicates a progressive but moderate degeneration of the sorbent's active sites, likely due to partial pore blockage or structural fatigue caused by repeated adsorption–desorption treatments. These results demonstrate that *C. japonica* powder combines high adsorption capacity with favorable regeneration ability and reusability as a biosorbent. Comparable gradual declines in removal efficiency over successive regeneration cycles have also been reported by other researchers, supporting the view that performance loss is common during repeated use of biosorbents [74].

3.13 Comparison of *C. japonica* powder efficiency with Plant-Based adsorbents

The adsorption capacity of *C. japonica* powder was compared with other plant-based adsorbents. Table 4 summarizes the adsorption capacity values obtained for various plant-derived adsorbents used in water treatment under comparable experimental conditions.

From the comparison, *C. japonica* powder used in this study recorded even higher dye adsorption capacity than some of other unmodified plant based adsorbents as shown

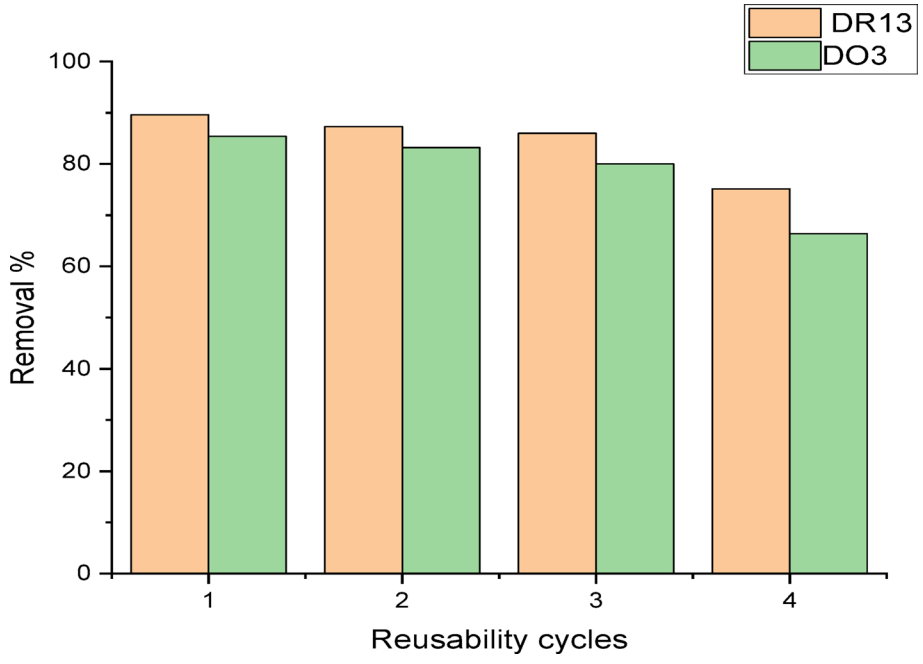

Fig. 10 Reusability cycles of the *C. japonica*

Table 4 Shows comparison of maximum uptake of dyes with various adsorbents

Adsorbent	Dye	Maximum adsorption capacity (mg/g)	Reference
Maize cob	Malachite green	66.52	[75]
Date seeds	Methyl violet	59.50	[76]
Rice husk	Methylene blue	24.48	[77]
Nut shell	Methylene blue	16.44	[78]
Cuscuta japonica	Disperse red 13	11.10	This study
Cuscuta japonica	Disperse orange 3	10.60	This study
Mango bark	Rhodamine	2.7	[79]
Sugar cane bagasse	Remazol Brilliant Violet-5R	2.45	[80]
Trifolium repens	Crystal violet	1.952	[81]
Gliricidia sepium	Disperse yellow 211	0.253	[82]

in Table 4. This makes the powder from *C. japonica* vines a suitable adsorbent for the removal of disperse dyes from water. It is worth noting that this is the first study to report the use of adsorbent derived from C. japonica for the removal of dyes from water.

3.14 Cost Estimation and analysis

Cuscuta japonica used in this study is an invasive plant abundantly available in the region, and was collected from the immediate surrounding environment at no cost. The preparation of the adsorbent, washing, drying, grinding, and acid treatment, was estimated to cost approximately USD 0.10 per kilogram under bench-scale conditions. Based on its adsorption capacity (q_e), the total treatment cost was calculated at about USD 0.025 per cubic metre of treated solution without adsorbent regeneration. This brought the total cost of the adsorbent to about USD 0.125 per kilogram. Besides, the adsorbent can be regenerated for reuse and therefore further reducing the cost. In comparison, the price of commercial activated carbon reported in the literature ranges between USD 1.20–6.40 per kilogram [83]. These findings indicate that *C. japonica* is a cost-competitive and sustainable alternative for dye removal compared to conventional adsorbents.

3.15 Novelty statement

This study reports for the first time the adsorption of disperse dyes onto the low cost powder obtained from *C. japonica* vines. Prior to this study, there were no reports for the possible utilization of this plant in the removal of dyes from water. Harnessing the invasive parasitic *C. japonica* is difficult, and therefore its utilization for the removal of dyes and other pollutants would be both of economic value and environmentally sustainable.

4 Conclusion

This study has shown that *C. japonica* powder can be effectively used to remove DR13 and DO3 from water through adsorption. DR13 exhibited higher removal efficiency (87.7%) compared to DO3 (79.16%) after 120 min. The adsorption process of the two dyes onto *C. japonica* powder followed the *pseudo*-second order kinetics suggesting a strong adsorbate-adsorbent interactions and is best described by the Sip isotherm model with DR13 achieving a slightly higher capacity (11.1 mg/g) than DO3 (10.6 mg/g). The removal efficiency of the two dyes by *C. japonica* decreased with increase in reaction temperature implying the reaction was exothermic in nature. The adsorption process

was feasible and spontaneous. Collectively, these findings highlight the potential of *C. japonica* powder as a renewable adsorbent for wastewater treatment. Beyond dye removal, valorizing this invasive plant as a treatment material provides a dual benefit of environmental remediation and ecological management offering a promising pathway toward sustainable water purification technologies.

Supplementary Information

The online version contains supplementary material available at https://doi.org/10.1007/s44371-025-00357-y.

Supplementary Material 1.

Acknowledgements
The authors acknowledge Masinde Muliro University of Science and Technology, Kenya for its support.

Author contributions
Authors Contributions: N.S, Methodology, Investigation, original draft preparation, R.K, Conceptualization, reviewed and edited the drafts and supervision, G.M, Conceptualization, reviewed and edited the drafts and supervision.

Funding
No funding was received for this study.

Data availability
Additional data to this manuscript is presented in the Supplementary Information.

Declarations

Ethics approval and consent to participate
Not Applicable.

Consent for publication
Not Applicable.

Competing interests
The authors declare no competing interests.

Received: 21 July 2025 / Accepted: 4 November 2025
Published online: 09 November 2025

References

1. Schandl H, Miatto A, Lenzen M, et al. Global material flows and resource productivity. The 2024 update. J Ind Ecol. 2024;28(6):1339. https://doi.org/10.1111/jiec.13593.
2. Kusumlata B, Kumar A, Gautam S. Sustainable solutions: reviewing the future of textile dye contaminant removal with emerging biological treatments. Limnological Rev. 2024;24(2):126. https://doi.org/10.3390/limnolrev24020007.
3. Keşkek Y, Yalçin Gürkan Y. Investigation of toxicological properties of some Azo dyes by Oecd Qsar method. Kırklareli Üniversitesi Mühendislik Ve Fen Bilimleri Dergisi. 2023;9(1):1. https://doi.org/10.34186/klujes.1242876.
4. Zewde D, Geremew B. Removal of congo red using Vernonia amygdalina leaf powder: optimization, isotherms, kinetics, and thermodynamics studies. Environ Pollutants Bioavailab. 2022;34(1):88. https://doi.org/10.1080/26395940.2022.2051751.
5. Islam MM, Aidid AR, Mohshin JN, et al. A critical review on textile dye-containing wastewater: Ecotoxicity, health risks, and remediation strategies for environmental safety. Clean Chem Eng. 2025;11:100165. https://doi.org/10.1016/j.clce.2025.100165.
6. Hübner U, Spahr S, Lutze H, et al. Advanced oxidation processes for water and wastewater treatment – Guidance for systematic future research. Heliyon. 2024;10(9):e30402. https://doi.org/10.1016/j.heliyon.2024.e30402.
7. Alaghemandi M. Sustainable solutions through innovative plastic waste recycling technologies. Sustainability. 2024;16(23):1. https://doi.org/10.3390/su162310401.
8. Azmi LS, Jabit N, Ismail S, et al. Membrane filtration technologies for sustainable industrial wastewater treatment: a review of heavy metal removal. Desalination Water Treat. 2025;323:101321. https://doi.org/10.1016/j.dwt.2025.101321.
9. Gkika DA, Tolkou AK, Katsoyiannis IA, Kyzas GZ. The adsorption-desorption-regeneration pathway to a circular economy: the role of waste-derived adsorbents on chromium removal. Sep Purif Technol. 2025;368:132996. https://doi.org/10.1016/j.seppur.2025.132996.
10. Ngeno EC, Mbuci KE, Necibi MC, et al. Sustainable re-utilization of waste materials as adsorbents for water and wastewater treatment in africa: recent studies, research gaps, and way forward for emerging economies. Environ Adv. 2022;9:100282. https://doi.org/10.1016/j.envadv.2022.100282.
11. Njewa JB, Shikuku VO. Recent advances and issues in the application of activated carbon for water treatment in africa: A systematic review (2007–2022). Appl Surf Sci Adv. 2023;18:100501. https://doi.org/10.1016/j.apsadv.2023.100501.
12. Ahmad Aftab R, Yusuf M, Ahmad F, et al. Green technology approach towards the removal of heavy Metals, Dyes, and phenols from water using Agro-based adsorbents: A review. Chem Asian J. 2024;19:1. https://doi.org/10.1002/asia.202400154.

13. Melhaoui R, Miyah Y, Kodad S, et al. On the suitability of almond shells for the manufacture of a natural Low-Cost bioadsorbent to remove brilliant green: kinetics and equilibrium isotherms study. Sci World J. 2021;2021. https://doi.org/10.1155/2021/665990.
14. Mihai S, Bondarev A, Călin C, Sîrbu EE. Adsorbent biomaterials based on natural clays and orange Peel waste for the removal of anionic dyes from water. Processes. 2024;12(5):1032. https://doi.org/10.3390/pr12051032.
15. Jadaa W. Wastewater treatment utilizing industrial waste fly Ash as a Low-Cost adsorbent for heavy metal removal: literature review. Clean Technol. 2024;6:221. https://doi.org/10.3390/cleantechnol6010013.
16. Chikri R, Elhadiri N, Benchanaa M, El maguana Y. Efficiency of sawdust as low-cost adsorbent for dyes removal. Hindawi J Chem. 2020. https://doi.org/10.1155/2020/8813420.
17. Bediako JK, Lin S, Sarkar AK, et al. Evaluation of orange peel-derived activated carbons for treatment of dye-contaminated wastewater tailings. Environ Sci Pollut Res. 2020;27(1):1053. https://doi.org/10.1007/s11356-019-07031-8.
18. Sahu S, Pahi S, Sahu JK, et al. Kendu (Diospyros melanoxylon Roxb) fruit Peel activated carbon—an efficient bioadsorbent for methylene blue dye: equilibrium, kinetic, and thermodynamic study. Environ Sci Pollut Res. 2020;27(18):22579. https://doi.org/10.1007/s11356-020-08561-2.
19. Sulyman M, Gierak A. Green environmental approach for adsorption of hazardous dye from water using tree and sea plant leaves (Dead L). Acta Sci Agric. 2020;4(2):01. https://doi.org/10.31080/ASAG.2020.04.766.
20. Iwuozor KO, Umeh CT, Sunday S, et al. A comprehensive review on the sequestration of dyes from aqueous media using maize- / corn-based adsorbents. Water Pract Technol. 2023;18(12):3065. https://doi.org/10.2166/wpt.2023.214.
21. Imran MS, Javed T, Areej I, Haider MN. Sequestration of crystal Violet dye from wastewater using low-cost coconut husk as a potential adsorbent. Water Sci Technol. 2022;85(8):2295. https://doi.org/10.2166/wst.2022.124.
22. Bulimo I, Mutua G, Owino J. Application of cuscuta Japonica powder as a Low-cost biosorbent for the removal of atrazine and diuron from aqueous solution: Kinetic, isothermal and thermodynamic studies. Dokl Phys Chem. 2024;517:83. https://doi.org/10.1134/S0012501625600044.
23. Ali A, Zhang N, Santos RM. Mineral characterization using scanning electron microscopy (SEM): A review of the Fundamentals, Advancements, and research directions. Appl Sci. 2023;13(23):12600. https://doi.org/10.3390/app132312600.
24. Iheanacho OC, Nwabanne JT, Obi CC, et al. Adsorptive dephenolization of aqueous solutions using thermally modified corn cob: Mechanisms, point of zero Charge, and isosteric heat studies. Adsorpt Sci Technol. 2023;2023. https://doi.org/10.1155/2023/2813663.
25. Kiteto MK, Mecha CA. Insight into the Bouguer-Beer-Lambert law: A review. Sustainable Chem Eng. 2024;5(2):567. https://doi.org/10.37256/sce.5220245325.
26. Guediri A, Bouguettoucha A, Tahraoui H, et al. The enhanced adsorption capacity of Ziziphus Jujuba stones modified with Ortho-Phosphoric acid for organic dye removal: A Gaussian process regression approach. Water. 2024;16(9):1208. https://doi.org/10.3390/w16091208.
27. Saidi M, Reguig BA, Amine Monir E, M., et al. Kinetics thermodynamics and adsorption study of Raw treated diatomite as a sustainable adsorbent for crystal Violet dye. Sci Rep. 2025;15(1):1. https://doi.org/10.1038/s41598-025-05787-3.
28. Reddy YS, Jose TJ, Dinesh B, et al. Equilibrium, kinetic, and thermodynamic study of direct yellow 12 dye adsorption by biomass-derived porous graphitic activated carbon. Biomass Convers Biorefinery. 2025;15(5):6817. https://doi.org/10.1007/s13399-024-05464-x.
29. Díaz E, García L, Ordóñez S. Adsorption of stable and labile emerging pollutants on activated carbon: degradation and mass transfer kinetic study. Appl Water Sci. 2024;14(4):1. https://doi.org/10.1007/s13201-023-02087-x.
30. Akhtar MS, Ali S, Zaman W. Innovative adsorbents for pollutant removal: exploring the latest research and applications. Molecules. 2024;29(18):1. https://doi.org/10.3390/molecules29184317.
31. Magdy A, Mostafa MR, Moustafa SA, et al. Kinetics and adsorption isotherms studies for the effective removal of Evans blue dye from an aqueous solution utilizing forsterite nanoparticles. Sci Rep. 2024;14:24392. https://doi.org/10.1038/s41598-024-73697-x.
32. Shikuku VO, Jemutai-Kimosop S. Efficient removal of sulfamethoxazole onto sugarcane bagasse-derived biochar: two and three-parameter isotherms, kinetics and thermodynamics. S Afr J Chem. 2020;73(1):111. https://doi.org/10.17159/0379-4350/2020/V73A16.
33. Mabuza MM, Mahlobo MGR. Adsorption equilibria and systematic thermodynamics analysis of carbon dioxide sequestration on South African coals using nonlinear Three-Parameter models: Sips, Tóth, and Dubinin–Astakhov. Energies. 2025;18(10):1. https://doi.org/10.3390/en18102646.
34. Pourbaba R, Abdulkhani A, Rashidi A, Ashori A. Lignin nanoparticles as a highly efficient adsorbent for the removal of methylene blue from aqueous media. Sci Rep. 2024;14(1):1. https://doi.org/10.1038/s41598-024-59612-4.
35. Khan SA, Manchanda A, Khan TA. Adsorption of coomassie brilliant blue on a novel Eco-Friendly nanogel from simulated water: Equilibrium, Kinetic, and thermodynamic studies. Chem Select. 2024;9(15):1. https://doi.org/10.1002/slct.202304927.
36. Thombare N, Mahto A, Singh D, et al. Comparative FTIR characterization of various natural gums: A criterion for their identification. J Polym Environ. 2023;31(8):3372. https://doi.org/10.1007/s10924-023-02821-1.
37. Feng N, She S, Tang F, et al. Formation and identification of Lignin-Carbohydrate complexes in Pre-hydrolysis liquors. Biomacromolecules. 2023;24(6):2541. https://doi.org/10.1021/acs.biomac.3c00053.
38. Hong T, Yin JY, Nie SP, Xie MY. Applications of infrared spectroscopy in polysaccharide structural analysis: Progress, challenge and perspective. Food Chemistry: X. 2021;12:100168. https://doi.org/10.1016/j.fochx.2021.100168.
39. Liu M, Li X, Li J, et al. Experimental study on the synergy between lignin and cellulose during co-torrefaction and its impact on the properties and structural characteristics of pyrolysis Biochar. Ind Crops Prod. 2025;224:120383. https://doi.org/10.1016/j.indcrop.2024.120383.
40. Jahin HS, Khedr AI, Ghannam HE. Banana peels as a green bioadsorbent for removing metals ions from wastewater. Discover Water. 2024;4(1):36. https://doi.org/10.1007/s43832-024-00080-2.
41. Belcaid A, Beakou BH, Bouhsina S, Anouar A. Insight into adsorptive removal of methylene blue, malachite green, and Rhodamine B dyes by cassava Peel Biochar (Manihot esculenta Crantz) in single, binary, and ternary systems: competitive adsorption study and theoretical calculations. Biomass Convers Biorefinery. 2024;14(6):7783. https://doi.org/10.1007/s13399-022-02928-w.

42. Ng HM, Omar FS, Kasi R, et al. Thermogravimetric analysis of polymers. Encyclopedia Polym Sci Technol. 2018. https://doi.org/10.1002/0471440264.pst667.
43. Pintor-ibarra LF, Alvarado-flores JJ, Rutiaga-quiñones JG, et al. Chemical and energetic characterization of the wood of prosopis laevigata: chemical and thermogravimetric methods. Molecules. 2024;29(11):2587. https://doi.org/10.3390/molecules29112587.
44. Rahman AA, Abdullah N. Characterization of treated empty fruit bunches by thermogravimetric analysis (TGA). E3S Web Conferences. 2025;603(1). https://doi.org/10.1051/e3sconf/202560301024.
45. Díez D, Urueña A, Piñero R, et al. Determination of Hemicellulose, Cellulose, and lignin content in different types of biomasses by thermogravimetric analysis and Pseudo-component kinetic model (TGA-PKM Method). Processes. 2020;8:1048. https://doi.org/10.3390/pr8091048.
46. Semwal N, Mahar D, Chatti M et al. (2023). Adsorptive removal of Congo Red dye from its aqueous solution by Ag–Cu–CeO_2 nanocomposites: Adsorption kinetics, isotherms, and thermodynamics *Heliyon*, *9*(11), e22027. https://doi.org/10.1016/j.heliyon.2023.e22027
47. Kayranli B. Adsorption efficiency of groundnut husk Biochar in reduction of Rhodamine B, recycle, and reutilization. Biomass Convers Biorefinery. 2025;15:25501. https://doi.org/10.1007/s13399-025-06781-5.
48. Pimentel CH, Freire MS, Gómez-Díaz D, González-Álvarez J. Removal of wood dyes from aqueous solutions by sorption on untreated pine (Pinus radiata) sawdust. Cellulose. 2023;30(7):4587–608. https://doi.org/10.1007/s10570-023-05145-4.
49. Sen TK. Adsorptive removal of dye (Methylene Blue) organic pollutant from water by pine tree leaf biomass adsorbent. Processes. 2023;11(7):1877. https://doi.org/10.3390/pr11071877.
50. Sudarsan S, Murugesan G, Varadavenkatesan T. Efficient adsorptive removal of congo red dye using activated carbon derived from Spathodea campanulata flowers. Sci Rep. 2025;15:1831. https://doi.org/10.1038/s41598-025-86032-9.
51. Arroussi A, Laksaci H, Djaafri M, et al. Effectiveness of plant-based biosorbents in textile dye removal from aqueous solutions: isotherm, kinetic, and thermodynamic studies. Comptes Rendus Chim. 2025;28:339. https://doi.org/10.5802/crchim.390.
52. Taylor P, Adam SH, Jalil AA, Triwahyono S. Novel removal of water-insoluble disperse dye onto a low-cost adsorbent prepared from tropical fruit waste. Desalination Water Treat. 2024;49(1–3):37. https://doi.org/10.1080/19443994.2012.719363.
53. Sriram G, Baby N, Dhanabalan K, et al. Studies of various batch adsorption parameters for the removal of Trypan blue using Ni-Zn-Bi-Layered triple hydroxide and their Isotherm, Kinetics, and removal mechanism. Inorganics. 2024;12:296. https://doi.org/10.3390/inorganics12110296.
54. de Costa C, Jurado-Davila LR, Oliveira IV, J. T., et al. Exploring key parameters in adsorption for effective fluoride removal: A comprehensive review and engineering implications. Appl Sci. 2024;14(5):2161. https://doi.org/10.3390/app14052161.
55. Haleem A, Shafiq A, Chen SQ, Nazar M. A comprehensive review on Adsorption, photocatalytic and chemical degradation of dyes and Nitro-Compounds over different kinds of porous and composite materials. Molecules. 2023;28(3):1081. https://doi.org/10.3390/molecules28031081.
56. Bounaas M, Bouguettoucha A, Chebli D, Derbal K, Benalia A. Effect of washing temperature on adsorption of cationic dyes by Raw lignocellulosic biomass. Appl Sci. 2024;14:10365. https://doi.org/10.3390/app142210365.
57. Tiwari M, Shukla SP, Mohan D, et al. Modified cenospheres as an adsorbent for the removal of disperse dyes. Adv Environ Chem. 2015;1. https://doi.org/10.1155/2015/349254.
58. Khamwichit A, Dechapanya W, Dechapanya W. Heliyon adsorption kinetics and isotherms of binary metal ion aqueous solution using untreated Venus shell. Heliyon. 2022;8:e09610. https://doi.org/10.1016/j.heliyon.2022.e09610.
59. Hassan MG, Wassel MA, Gomaa HA, Elfeky AS. Adsorption of Rose Bengal dye from waste water onto modified biomass. Sci Rep. 2023;13(1):1. https://doi.org/10.1038/s41598-023-41747-5.
60. Kikuvi J, Mutua G, Gembo RO, Orata F. Kinetic, isothermal and thermodynamic study on the adsorptive removal of Chloramphenicol from water by iron – impregnated Kenyan clinoptilolite zeolite. Reaction Kinetics Mech Catal. 2025;138:3205. https://doi.org/10.1007/s11144-025-02876-2.
61. Sudrajat H, Susanti A, Putri DKY, Hartuti S. Mechanistic insights into the adsorption of methylene blue by particulate Durian Peel waste in water. Water Sci Technol. 2021;84(7):1774. https://doi.org/10.2166/wst.2021.361.
62. Musah M, Mathew JT, Azeh Y, et al. Intraparticle diffusion study of the adsorption of Ni^{2+} and Mn^{2+}. Dev J Sci Technol Res. 2023;13(1):73.
63. Sangoremi AA. Adsorption kinetic models and their applications: A critical review. Int J Res Sci Innov. 2025;XIIV:245. https://doi.org/10.51244/ijrsi.2025.120500019.
64. Hasani N, Selimi T, Mele A, et al. Theoretical, Equilibrium, kinetics and thermodynamic investigations of methylene blue adsorption onto lignite coal. Molecules. 2022;27(6):1856. https://doi.org/10.3390/molecules27061856.
65. Hoa NTH, Quynh NT, Nguyen VD, et al. Adsorptive removal of reactive black 5 by Longan Peel-Derived activated carbon: Kinetics, Isotherms, Thermodynamics, and modeling. Water. 2025;17(11):1. https://doi.org/10.3390/w17111678.
66. Shahat A. Removing atrazine herbicide from water with an efficient metal-organic framework. Appl Organomet Chem. 2024;38(2):e7334. https://doi.org/10.1002/aoc.7334.
67. Ehiomogue P, Ahuchaogu II, Ahaneku IE. Review of adsorption isotherms models. Acta Technica Corviniensis. 2022;14(4):87.
68. Al-saeedi SI, Ashour M. Adsorption of toxic dye using red seaweeds from synthetic aqueous solution and its application to industrial wastewater effluents. Front Mar Sci. 2023;10:1202362. https://doi.org/10.3389/fmars.2023.1202362.
69. AlJaberi FY. Extensive study of Electrocoagulation-Based adsorption process of real groundwater treatment: isotherm Modeling, adsorption Kinetics, and thermodynamics. Water. 2024;16(4):619. https://doi.org/10.3390/w16040619.
70. Çiçekçi A, Sevim F, Sevim M, Kavcı E. Adsorption Capacity, reaction kinetics and thermodynamic studies on Ni(II) removal with GO@Fe_3O_4@Pluronic-F68 nanocomposite. Polymers. 2025;17(15):1. https://doi.org/10.3390/polym17152141.
71. Sajjadi SM. Evaluation of the various adsorption isotherm models for the photocatalytic removal of methylene blue from the wastewater by graphene oxide / TiO_2 / SiO_2. Journal Appl Res Water Wastewater. 2024;11(1):59. https://doi.org/10.22126/arww.2023.8980.1286.
72. Al-asadi ST. Adsorption of methylene blue dye from aqueous solution using low cost adsorbent: Kinetic, isotherm adsorption and thermodynamic studies. Environ Monit Assess. 2023;195:676.
73. Ismail BM, Zayed AM, Roshdy MA, et al. Statistical modeling of mutagenic Azo dye adsorption on Bagasse activated carbon. Sci Rep. 2025;15:20112.

74. Othman JAS, Ngadi N, Ilyas RA, et al. Development and characterization of magnetic polyethyleneimine-bamboo nanocellulose adsorbents for enhanced performance of dye pollutant removal. Bioresources Bioprocess. 2025;12:86. https://doi.org/10.1186/s40643-025-00928-y.
75. Ojediran JO, Dada AO, Aniyi SO, et al. Mechanism and isotherm modeling of effective adsorption of malachite green as endocrine disruptive dye using acid functionalized maize cob (AFMC). Sci Rep. 2021;11(1):1. https://doi.org/10.1038/s41598-021-00993-1.
76. Ali NS, Jabbar NM, Alardhi, et al. Adsorption of Methyl Violet dye onto a prepared bio-adsorbent from date seeds: isotherm, kinetics, and thermodynamic studies. Heliyon. 2022;8(8):e10276. https://doi.org/10.1016/j.heliyon.2022.e10276.
77. Quansah JO, Hlaing T, Lyonga FN, et al. Nascent rice husk as an adsorbent for removing cationic dyes from textile wastewater. Appl Sci. 2020;10(10):3437. https://doi.org/10.3390/app10103437.
78. Ykhlef L, Ghania H, Salah H. Kinetic and adsorption equilibrium studies for removal of textile dye from aqueous solutions on nut shell adsorbent. Cellul Chem Technol. 2024;58(9–10):1135. https://doi.org/10.35812/CelluloseChemTechnol.2024.58.97.
79. Vara D, Jha S, Bisht S et al. (2024). Sustainable Bio-Based Adsorbents for Simultaneous and Efficient Removal of Hazardous Dyes from Aqueous Solutions. *Toxics*, 1;12(4), 266. https://doi.org/10.3390/toxics12040266
80. Ullah T, Gul H, Khitab F, et al. Adsorption of remazol brilliant Violet-5R from aqueous solution using sugarcane Bagasse as biosorbent: kinetic and thermodynamic studies. Water. 2022;14:3014. https://doi.org/10.3390/w14193014.
81. Gul S, Afsar S, Gul H, Ali B. Removal of crystal Violet dye from wastewater using low-cost biosorbent trifolium repens stem powder. J Iran Chem Soc. 2023;20(11):2781. https://doi.org/10.1007/s13738-023-02875-x.
82. Oluwasola AT, Labunmi L, Joseph OB, et al. Adsorption potential of gliricidia sepium on disperse yellow 211 dye. Am J Chem Appl. 2018;5(3):40.
83. Shaheen J, Fseha YH, Sizirici B. Heliyon Performance, life cycle assessment, and economic comparison between date palm waste Biochar and activated carbon derived from Woody biomass. Heliyon. 2022;8(12):e12388. https://doi.org/10.1016/j.heliyon.2022.e12388.

Publisher's note